Doc.No.: SPIN-UB-ATBD-1.02
Version: 1.02
Date: March 24, 2013

ESA SPARC Initiative – SPIN

Algorithm Theoretical Baseline Document

– ATBD –

Version 1.02

Adam Bourassa[2]
Greg Bodeker[3]
Lena Brinkhoff[1]
John Burrows[1]
Erkki Kyrölä[4]
Patricia Liebing[1]
Landon Rieger[2]
Joachim Urban[5]
Katja Weigel[1]

[1] Institute of Environmental Physics, University of Bremen, Germany
[2] Institute for Space and Atmospheric Sciences, University of Saskatchewan, Canada
[3] Bodeker Scientific, Alexandra, New Zealand
[4] Finnish Meteorological Institute, Helsinki, Finland
[5] Department of Earth and Space Sciences, Chalmers University of Technology, Gothenburg, Sweden

March 24, 2013

Contents

Document Properties

Reference	SPIN-UB-ATBD-1.02
Issue	1.02
Revision	00
Status	Draft
Date of issue	March 24, 2013
Document type	Deliverable

	Function	Name	Date
Lead author	Deliverable Coordinator	Patricia Liebing	March 24, 2013
Contributing authors	WP authors	Adam Bourassa Greg Bodeker Lena Brinkhoff John Burrows Erkki Kyrölä Landon Rieger Joachim Urban Katja Weigel	
Reviewed by			
Approved by			
Issued by			

Change Record and Distribution List

Document Change Log

Version	Date	Section/Page	Description
Draft 1.00	August 23, 2012	all	new document
Draft 1.01	September 19, 2012	7.1, 7.2 1 author list	added minor changes added J. Urban
Draft 1.02	March 24, 2013	3.1 2 3.1 3.1 3.1.2.3 3.1.4 6.1 6.1.1 6.1.13 6.1.12 5.1 5.1.2.1(3) 4.1 8	added description of ATBD principle added data version 7.03→7.04 Eqs. 3.4, 3.6 updated Henyey-Greenstein part replaced by Mie phase function description added added version number added influence of different L1 versions added error estimates added figure 6.1 updated text, added fig. 5.1 removed added/changed first 2 paragraphs added

Distribution List

- ESA

1 Introduction

This document was prepared by the SPIN consortium as deliverable D6 of the ESA SPARC Initiative (SPIN) project. The main scope of this project is to make use of ESA and ESA Third-Party Mission data to establish climate quality stratospheric data records from satellite instruments for the four essential climate variables of ozone, aerosol, water vapor and temperature in the stratosphere. The document aims at the facilitation of the use of these data products.

This work is supported by the European Space Agency.

1.1 Purpose and Scope

Algorithm Theoretical Baseline Documents (ATBD) were originally created within NASAs Earth Observing System. The approach has been accepted by all relevant space agencies. ATBDs are intended to describe the physical background or theory, the mathematical foundation and inversion techniques used to derive data products. All assumptions applied to the data are explained and justified. In general, ATBDs are written for different levels of product e.g. level 0 to 1, level 1 to 2 etc. The levels of data product are defined as follows: Level 0 data are raw instrument data, often in engineering units, as recorded by the instrument. Level 1 data are related variables after the application of a raw signal to the measurement algorithm, e.g. radiance at the top of the atmosphere. Level 2 data are the geophysical variables, e.g. trace gas or aerosol profiles at a given location and time of the observation. Level 3 data (products) usually take the form of a homogeneous regularly gridded field. Level 4 data are products derived from further processing and consolidation of Level 3 data (value-adding). The geophysical quantities are then available to the scientific community for studies of the various characteristics of the Earth system. The ATBD approach was developed to meet the need of the entire user community to assess the information content of a data product, its precision and accuracy.

In the context of the SPIN project. the Algorithm Theoretical Baseline Document describes the algorithms used within the various work packages of the SPIN project to generate the delivered data products. This comprises the specification of the data sets used, the description of the applied filtering and processing steps and of the theoretical assumptions or model parameters involved in the algorithms. It also contains an uncertainty assessment where possible. It does not include the algorithms to obtain the input data such as the calibrated data from satellite instruments.

The document is structured into four chapters for each climate variable considered within the project. Each section contains the description of the algorithm for one particular deliverable data product.

2 Scientific Background and Motivation

The scientific objective of the SPIN project is to characterize or extent existing and to establish new Climate Data Records (CDR) for four essential variables in the stratosphere (ozone, water vapor, temperature and aerosols). The explicit goal of SPIN is to make use of ESA and ESA Third Party missions (TPM) in order to continue and complement the CDRs so far obtained mainly using data by US (NASA and NOAA) missions.

CDRs usually contain a synergy of observations by several instruments combined in such a way that instrument specific errors are minimized and spatial and temporal coverage is optimized. While the SPARC CDRs currently rely heavily on data from solar occultation instruments which were operational until around 2005, the inclusion of ESA and ESA-TPM mission data will not only extent these CDRs in time but also by numerous novel measurement techniques. These include limb scatter observations in a wide spectral range (SCIAMACHY and OSIRIS, bright limb observations by GOMOS) as well as stellar occultation technique (GOMOS). The addition of these new data therefore significantly improves the spatio-temporal coverage of the CDRs.

The use of these new measurement techniques requires the application of novel analysis methods in order to account for complications due multiple scattering in limb observations or scintillations in stellar occultation measurements. Therefore, a considerable amount of time during phase 1 of the project will be assigned to the investigation and maturation of data products obtained from such measurements.

This Algorithm Theoretical Baseline document will describe the algorithms applied to obtain the matured individual data sets and the revised or new climatologies of stratospheric temperature and short lived species as outlined in Task 2 as well as the procedures used to obtain the merged data sets within Tasks 3 and 4 of the project.

Within the first phase of SPIN this comprises the description of the matured SCIAMACHY and OSIRIS aerosol data, the SCIAMACHY water vapor product and the GOMOS bright limb ozone product. The generation of stratospheric temperature climatologies for ACE-FTS, MIPAS, SMR and radio occultation data and of climatologies for short lived species are outlined here as well. Within phase 2 of SPIN the data sets of stratospheric temperature and ozone are to be compared to and merged with historical data records to create long term climatologies. In addition, a path to merging climatologies for aerosols (including the limb scatter data) and water vapor with the corresponding historical records based on extensive comparison studies is to be outlined.

3 Algorithm Theoretical Baseline – Aerosol

3.1 Algorithms for the Maturation of Aerosol Products – SCIAMACHY (WP–12)

This section is adapted from Ernst et al. (2012).

The retrieval of stratospheric aerosols is based on SCIAMACHY Level 1 data version 7.04. The Level 1 data are calibrated with all calibration options but flags 0, 6, and 7, i.e., memory effect correction, polarization correction and absolute calibration were not performed due to remaining issues with these calibration steps.
The stratospheric aerosol extinction profiles are retrieved from SCIAMACHY limb-radiance profiles at two wavelengths using a color-index approach. The two wavelengths are $\lambda_s = 470$ nm and $\lambda_l = 750$ nm. Spectral windows with weak atmospheric absorption are selected in order to avoid retrieval errors caused by incorrect knowledge of absorber profiles. Both wavelengths used are sufficiently distant from the center of the Chappuis absorption band of O_3 near 600 nm. λ_s falls between an NO_2 and the Chappuis absorption band, and λ_l is just below the O_2 A-band. The measurement vector required for the retrieval is derived from the limb-radiance profiles at the two wavelengths using a 2-step approach following the method previously used by Bourassa et al. (2007).
First we normalize the limb-radiance at each tangent height with the radiance at a reference tangent height of the same limb-radiance profile:

$$I_N^\lambda(TH) = I^\lambda(TH)/I^\lambda(TH_{ref}) \tag{3.1}$$

This technique is adapted from trace gas retrievals (e.g., Flittner et al., 2000; von Savigny et al., 2003). It has two advantages: first, an absolute calibration of the limb-radiances is not required. Furthermore, von Savigny et al. (2003) showed that the tangent height normalization leads to a reduced sensitivity to errors in the assumed ground albedo. This is based on the assumption that the fraction of ground-reflected sunlight in the limb-radiance is similar at all tangent heights, including the reference tangent height. A reference tangent height (TH_{ref}) of about 35 km is chosen because at this point (and above) the aerosol loading in the atmosphere is small under background conditions. Above that tangent height the SCIAMACHY limb measurements are potentially contaminated by external or "baffle" stray light.

In a second step we combine the normalized limb-radiance profiles at the two wavelengths in a color-index-ratio. Retrieving aerosol extinction profiles from limb-radiance profiles at a single wavelength is also an option, but it relies on the assumption that the background Rayleigh atmosphere can be modeled perfectly. Any uncertainty in the neutral density would result in an error in the aerosol profile. To reduce this effect, it is suitable to use the ratio of a long to a short wavelength. Since the Ångstrøm exponent for Mie-scattering is highly variable – but for stratospheric aerosols generally significantly smaller than for Rayleigh scattering ($\alpha \approx 4$) – wavelength pairing provides a suitable measurement vector for the retrieval of stratospheric aerosols. Instead of the simple ratio of the two normalized limb-radiance profiles, we use the natural logarithm of the ratio as the retrieval vector for the inversion (see below). The wavelength pairing can then be described mathematically as follows:

$$y(TH) = \ln\left(\frac{I_N^{\lambda_l}(TH)}{I_N^{\lambda_s}(TH)}\right) \tag{3.2}$$

Obtaining stratospheric aerosol extinction coefficient profiles from SCIAMACHY limb-radiance profiles is an inverse problem, requiring the inversion of the following generic equation:

$$\mathbf{y} = \mathbf{K}\mathbf{x} + \epsilon, \tag{3.3}$$

where $\mathbf{y}$ is the measurement vector containing logarithms of the normalized and paired limb-radiance profiles at each selected tangent height – as described above. $\mathbf{x}$ is the so-called state vector, representing the height distribution of the desired atmospheric parameter, i.e., in this case the aerosol extinction coefficient at each altitude. $\mathbf{K}$ is the weighting function matrix or Jacobian matrix which contains logarithmic weighting functions for the aerosol extinction coefficient at tangent heights from about 11.5 km to 31.5 km (tangent height numbers 6 to 12). ϵ contains all errors. In order to solve the inversion problem we employ the optimal estimation technique – briefly described in the following Sect. 3.1.1 – in combination with the radiative transfer model SCIATRAN – described in Sect. 3.1.2.

3.1.1 Retrieval technique

In SCIATRAN, Eq. (3.3) is used in form of

$$\hat{\mathbf{y}} = \mathbf{K}\hat{\mathbf{x}} + \epsilon, \tag{3.4}$$

where $\hat{\mathbf{y}} = \mathbf{y} - \mathbf{y_0}$ is the measurement vector containing the differences between logarithms of measured and simulated spectra (both normalized and paired) and $\hat{\mathbf{x}} = (\mathbf{x} - \mathbf{x_0})/\mathbf{x_0}$ is the state vector containing relative differences between the a priori and retrieved aerosol extinction profiles. Following Rodgers (2000), the solution of Eq. (3.4) is found as

$$\mathbf{x} = \mathbf{x}_0 + (\mathbf{K^T}\mathbf{S_y^{-1}}\mathbf{K} + \mathbf{S}_a^{-1})^{-1}\mathbf{K^T}\mathbf{S_y^{-1}}(\mathbf{y} - \mathbf{y}_0)\mathbf{x}_0 \tag{3.5}$$

with $\mathbf{S}_\mathrm{a}$ as the a priori covariance matrix and $\mathbf{S}_\mathrm{y}$ as the noise covariance matrix. Because of the non-linearity of the problem, the forward model and retrieval code SCIATRAN version 3.1 (Rozanov et al., 2005) is used to find the solution iteratively:

$$\mathbf{x}_{i+1} = \mathbf{x}_i + (\mathbf{K^T}_i\mathbf{S}_y^{-1}\mathbf{K}_i + \mathbf{S}_a^{-1})^{-1}\mathbf{K^T}_i\mathbf{S}_y^{-1}(\mathbf{y} - \mathbf{y}_i)\mathbf{x}_i \tag{3.6}$$

with $\mathbf{S}_\mathrm{i} = (\mathbf{K^T}_\mathrm{i}\mathbf{S}_\mathrm{y}^{-1}\mathbf{K}_\mathrm{i} + \mathbf{S}_\mathrm{a}^{-1})^{-1}$ as the solution covariance matrix.
The noise covariance matrix is chosen to be diagonal, i.e., the errors are assumed to be uncorrelated. A signal to noise ratio of 200 is used for all tangent heights and spectral points. In terms of the a priori covariance matrix the non-diagonal elements drop off exponentially with a correlation radius of 3.3 km and the diagonal elements correspond to a relative standard deviation of 1.

3.1.2 Input to the retrieval

3.1.2.1 SCIATRAN

SCIATRAN is a linearized radiative transfer model designed to simulate the scattered solar radiation and the weighting functions of various atmospheric parameters in the UV-Visible-near-IR spectral range for any viewing geometry (nadir, zenith, off-axis, limb, etc.) and any observer position within and outside the atmosphere. The software package also contains a retrieval algorithm, which can be easily adjusted to solve a wide range of scientific tasks. For the retrieval of aerosols from SCIAMACHY limb-measurements, the discrete ordinate solver of SCIATRAN 3.1 (Rozanov et al., 2005) was used. SCIATRAN allows for a field of view integration to take the finite vertical resolution of the SCIAMACHY limb-measurements into account. The retrieval altitude grid is a regular 1 km grid.

3.1.2.2 Auxiliary Data

The albedo values are taken from the Matthews data base (Matthews, 1983) and the temperature and pressure profiles for the location, date and time at each limb measurement are taken from the ECMWF Operational Atmospheric Model Data Sets.
The wavelength dependence of the aerosol extinction coefficient is determined by the assumed aerosol model. Trace gases are not considered.

3.1.2.3 Aerosol parameterization in SCIATRAN

For the retrieval, Version 1.1, the needed parameters are delivered manually to SCIATRAN by using a Mie phase function. As discussed among others by Deshler (2008), for background stratospheric aerosols the dominating smaller particle mode can be described by the lognormal size distribution with a median radius of r = 0.11 μm and a distribution width of $\sigma = 1.37$. These parameters have been adopted to calculate the aerosol phase function using a Mie code. In accordance to Yue et al. (1994) the real part of the refractive index of aerosol particles has been set to $n_r = 1.453$ at 450 nm and to $n_r = 1.446$ at 800 nm, while the imaginary part of $n_i = 10^{-8}$ has been used for both wavelengths.

3.1.2.4 A priori aerosol extinction profiles

The a priori aerosol extinction profiles required for the retrievals are determined with the ECSTRA model by Fussen and Bingen (1999). ECSTRA is a climatological model of vertical extinction coefficient profiles of stratospheric aerosols in the UV-Visible range as a function of wavelength, month, latitude, and volcanism level represented by the aerosol optical depth. The ECSTRA model is based on SAGE II stratospheric aerosol extinction profile data. ECSTRA provides aerosol extinction profiles above the tropopause only, and the tropopause height is taken – depending on latitude and month of the year – from the climatological tropopause height data set by Randel et al. (2000). The vertical structure of the ECSTRA aerosol profile climatology describes the tropopause region, the Junge layer and the high altitude domain (Fussen and Bingen, 1999).
The ECSTRA aerosol extinction profiles are extrapolated exponentially above 30 km with a scale height of 4 km, based on Thomason et al. (2006), and we remove the edge below the tropopause that is generated by the ECSTRA model.

3.1.3 Output

The retrieval output is the aerosol extinction coefficient at $\lambda_s = 470$ nm and $\lambda_l = 750$ nm for each tangent height in 1 km steps.

3.1.4 Error

The main error source of the retrieval Version 1.0 was the aerosol phase function, which has been improved in Version 1.1. A sensitivity study for the median radius of the phase function showed a maximum relative error in the retrieved aerosol extinction coefficients of - 100% for large radii (relative to r = 0.11 m) at the equator and + 100% to + 200% for very small radii in the southern hemisphere. Further potential error sources of Version 1.1 were tested by means of synthetic retrievals. The effect on the retrieved aerosol extinction of a ± 15% uncertainty in the ozone profile is below 1% for both a polar and tropical geometry. For a typical SCIAMACHY tangent height error of ± 200 m (von Savigny et al., 2009), the maximum error is 8% at 16 km and smaller than 5% above 20 km. The error due to uncertainties in the assumed surface albedo is up to 30% (at 40°S) when changing the true albedo from 0 to 1 and running the retrieval with A = 0.5. However, the application of a cloud screening – assuming tropospheric clouds below the SCIAMACHY measurement to be a major source for albedo uncertainties – does not improve the retrieval (see Ernst et al. (2012)). Furthermore, changing the

true neutral density by ± 3% by scaling the ground pressure of 1013 hPa by ± 30 hPa has an effect on the retrieved aerosol extinction, which is smaller than 20% below 20 km and smaller than 5% above. Finally, the impact of the a priori profile on the retrieval result has been analysed. The relative error due to the a priori profile using 6 modifications – multiplication with a factor of 0.5 and 2, a height shift of the complete profile by ± 3 km, and an artificial maximum and minimum around an altitude of 25 km – is smaller than 10%.

Bibliography

Bourassa, A. E., Degenstein, D. A., Gattinger, R. L., and Llewellyn, E. J., Stratospheric aerosol retrieval with optical spectograph and infrared imaging system limb scatter measurements, J. Geophys. Res., 112, D10217, 2007.

Deshler, T.: A review of global stratospheric aerosol: Measurement, importance, life cycle, and local stratospheric aerosol, Atmos. Res., 90, 223–232, doi:10.1016/j.atmosres.2008.03.016, 2008.

Ernst, F., von Savigny, C., Rozanov, A., Rozanov, V., Eichmann, K.-U., Brinkhoff, L. A., Bovensmann, H., and Burrows, J. P., Global stratospheric aerosol extinction profile retrievals from SCIAMACHY limb-scatter observations, Atmos. Meas. Tech. Discuss, 5, 5993–6035, 2012.

Flittner, D. E., Bhartia, P. K., and Herman, B. M., O3 profiles retrieved from limb scatter measurements: Theory, Geophys. Res. Lett., 27(17), 2601–2604, doi:10.1029/1999GL011343, 2000.

Fussen, D. and Bingen, C., A volcanism dependent model for the extinction profile of stratospheric aerosols in the UV-visilble range, Geophys. Res. Lett., 26(6), 703–706, 1999.

Matthews, E., Global vegetation and land use: new high resolution data base for climate studies, J. Climate Appl. Meteor., 22, 474–487, 1983.

Randel, W., Wu, F., and Gaffen, D., Interannual variability of the tropical tropopause derived from radiosonde data and NCEP reanalyses, J. Geophys. Res., 105(D12), 15509–15523, 2000.

Rodgers, C. D., Inverse Methods for Atmospheric Sounding: Theory and Practice, World Scientific, Singapore, 2000.

Rozanov, A., Rozanov, V., Buchwitz, M., Kokhanovsky, A., and Burrows, J. P., SCIATRAN 2.0 - A new radiative transfer model for geophysical applications in the 175–2400 nm spectral region, Adv. Space Res. 36(5), 1015–1019, doi:10.1016/j.asr.2005.03.012, 2005.

von Savigny, C., Haley, C. S., Sioris, C. E., McDade, I. C., Llewellyn, E. J., Degenstein, D., Evans, W. F. J., Gattinger, R. L., Griffioen, E., Kyrölä, E., Lloyd, N. D., McConnell, J. C., McLinden, C. A., Mégie, G., Murtagh, D. P., Solheim, B., and Strong, K., Stratospheric ozone profiles retrieved from limb scattered sunlight radiance spectra measured by the OSIRIS instrument on the Odin satellite, Geophys. Res. Lett., 30(14), 1755, doi:10.1029/2002GL016401, 2003.

von Savigny, C., Bovensmann, H., Bramstedt, K., Dikty, S., Ebojie, F., Jones, A., Noël, S., Rozanov, A., and Sinnhuber, B.-M.: Indications for long-term trends and seasonal variations in the SCIAMACHY Level 1 version 6.03 tangent height information, SCIAMACHY Technical Note, TN-IUP-scia-pointing-2009-01, University of Bremen, Bremen, 2009.

Thomason, L.W., Peter, Th., Carslaw, K. S., Kärcher, B., Notholt, J., Bingemer, H., Hamill, P., Brogniez, C., Deshler, T., Anderson-Sprecher, R., Weisenstein, D. and Bekki, S., SPARC Assessment of Stratospheric Aerosol Particles, World Climate Research Programme (WCRP) SPARC Project Report (4), 1–320, 2006.

Yue, G. K., Poole, L. R., Wang, P.-H., and Chiou, E. W.: Stratospheric aerosol acidity, density, and refractive index deduced from SAGE II and NMC temperature data, J. Geophys. Res., 99(D2), 3727–3738, doi:10.1029/93JD02989, 1994.

3.2 Algorithms for the Maturation of Aerosol Products – OSIRIS (WP–12)

This algorithm theoretical basis document describes the retrieval of stratospheric aerosol extinction and Ångström coefficients on a scan-by-scan basis using the limb scatter OSIRIS instrument (*Llewellyn et al.*, 2004) onboard the Odin satellite.

3.2.1 Algorithm Overview

Currently, stratospheric aerosol extinction is retrieved by OSIRIS using a single 750 nm measurement vector and a multiplicative algebraic reconstruction technique (MART) as described in detail by *Bourassa et al.* (2007, 2011). For these retrievals a lognormal particle size distribution of the form,

$$\frac{dn(r)}{dr} = \frac{n_{\text{aer}}}{r\ln(\sigma_g)\sqrt{2\pi}} \exp\left(-\frac{(\ln r - \ln r_g)^2}{2\ln(\sigma_g)^2}\right), \tag{3.7}$$

is assumed with a mode radius, r_g, of 80 nm and mode width, σ_g, of 1.6, as is typical of stratospheric aerosol during volcanically quiescent periods (*Deshler et al.*, 2003). The number density, n_{aer}, is then retrieved and converted to extinction to decrease the dependence on the particle size assumptions. While extinction is much less sensitive to the assumed parameters (*McLinden et al.*, 1999), error in the assumed size distribution still biases the retrieved extinction. This work seeks to extend the current algorithm to retrieve an estimate of aerosol particle size and improve the retrieved extinction.

The aerosol signal detected by a limb scatter instrument is highly wavelength dependent and incorporation of this dependence can be used to improve the determination of aerosol extinction as well as retrieve information about particle microphysics. This technique uses OSIRIS measurements at two wavelengths, 750 nm and 1.53 μm to retrieve two parameters of a unimodal lognormal distribution, the number density and mode radius. These are then converted to a 750 nm aerosol extinction and the Ångström coefficient to decrease the dependence on particle size assumptions. Inversion of the OSIRIS measurements are performed using SASKTRAN, a fully spherical multiple scattering radiative transfer model (*Bourassa et al.*, 2008), to iteratively compute the atmospheric state.

3.2.2 The Aerosol Measurement Vector

To maximize the sensitivity to aerosols the radiance measurements, I, are first normalized in log space by a modeled measurement, I_{Ray}, in a clean, aerosol free atmosphere.

$$y_j(\lambda) = \ln\left(\frac{I(\lambda, j)}{I_{\text{Ray}}(\lambda, j)}\right). \tag{3.8}$$

To minimize the sensitivity of the aerosol measurement to an unknown surface albedo and tropospheric clouds and eliminate the need for an absolute calibration, the radiance measurements are then normalized by one or more high altitude measurements (*von Savigny et al.*, 2003). To select altitudes which are above the bulk of the aerosol layer and below altitudes which are contaminated by stray light, altitudes are chosen in which the measurement vector given by Equation 3.8 is at a minimum. Any altitudes with a measurement vector within 0.01 of the minimum are then used for normalization. This provides the final measurement vector,

$$y_j(\lambda) = \ln\left(\frac{I(\lambda, j)}{I_{\text{Ray}}(\lambda, j)}\right) - \frac{1}{N}\sum_{j=m}^{m+N} \ln\left(\frac{I(\lambda, j)}{I_{\text{Ray}}(\lambda, j)}\right), \tag{3.9}$$

where N lines-of-sight, from tangent altitude $j = m$ to $m+N$ are used in the normalization. Typically, this results in normalization between 35 and 40 km in the tropics, extending to lower altitudes at higher latitudes (*Bourassa et al.*, 2011).

3.2.3 Aerosol Inversion

3.2.3.1 Albedo retrieval and MART Initialization

The OSIRIS version 5 aerosol algorithm (*Bourassa et al.*, 2011) is used as the *a priori* estimate of aerosol extinction and particle size for the improved retrieval. First, an effective Lambertian surface albedo must be retrieved due to the strong effect of albedo on the retrieved aerosol. Albedo is retrieved by modeling the 750 nm OSIRIS signal at the normalization altitude for albedo values of 0, 0.25, 0.5, 0.75 and 1 using the *a priori* aerosol values. The modeled radiances are then linearly interpolated from the nearest modeled values to find the retrieved albedo.

The aerosol number density is then retrieved using the MART technique (*Lloyd and Llewellyn*, 1989) assuming a single mode lognormal particle size distribution with a mode radius of 80 nm and mode width of 1.6. For this, an *a priori* aerosol profile is chosen with very low values at all altitudes to ensure the Jacobian is positive and to maximize the retrieval range. At each iteration the aerosol number density at altitude j is updated based on the ratio of the measurement, y, to the model, $F(\hat{\mathbf{x}}^{(n)}, \tilde{\mathbf{b}})$,

$$\hat{x}_i^{(n+1)} = \hat{x}_i^{(n)} \sum_j \frac{y_j}{F_j(\hat{\mathbf{x}}^{(n)}, \tilde{\mathbf{b}})} W_{ji}. \tag{3.10}$$

For the aerosol retrieval, the weighting matrix, $\mathbf{W}$, is simply the identity matrix and MART simplifies to a Chahine relaxation (*Chahine*, 1970, 1972). Ten iterations are performed to ensure convergence. Albedo is then re-retrieved and then aerosol is again retrieved with ten iterations using the updated albedo. This provides a stable albedo and aerosol product with further iterations typically changing albedo by less than 1%.

3.2.3.2 Coupled Extinction and Particle Size Retrieval

Although three parameters are required to fully describe the lognormal distribution only two independent measurements are taken, requiring the mode width to be assumed constant at 1.6. The number density and mode radius are then the two quantities which are retrieved. Solving for the atmospheric state is equivalent to searching the two dimensional solution space for the point which minimizes the difference between the model and the measurements. There are several possible methods for this, however for multidimensional non-linear problems Levenberg-Marquardt is often used, as it provides a good combination of speed and robustness (*Marquardt*, 1963). Each iteration of the atmospheric state at altitude j is then given by

$$\hat{x}_j^{(n+1)} = \hat{x}_j^{(n)} + \left(\mathbf{K}_j^{\mathrm{T}}\mathbf{K}_j + \gamma \mathrm{diag}(\mathbf{K}_j^{\mathrm{T}}\mathbf{K}_j)\right)^{-1} \mathbf{K}_j^{\mathrm{T}} \left(y_j - F_j(\hat{\mathbf{x}}^{(n)}, \tilde{\mathbf{b}})\right). \tag{3.11}$$

Jacobian Calculation

The Jacobian, $\mathbf{K}$ for each line-of-sight is assumed to be independent, with no altitude coupling. While possible to compute the full Jacobian with altitude coupling terms, the computational time is prohibitive and for long wavelengths the altitude coupling is relatively small. Inclusion is then unnecessary for convergence and the Jacobian for a particular altitude, j, can be written,

$$\mathbf{K}_j = \begin{pmatrix} \dfrac{\partial y_j(750\,nm)}{\partial r_g} & \dfrac{\partial y_j(750\,nm)}{\partial n_{\mathrm{aer}}} \\ \dfrac{\partial y_j(1.53\mu m)}{\partial r_g} & \dfrac{\partial y_j(1.53\mu m)}{\partial n_{\mathrm{aer}}} \end{pmatrix}. \tag{3.12}$$

Calculation of the Jacobian is performed numerically at each iteration by successively perturbing the entire aerosol number density and mode radius profiles by 5% and recomputing the measurement vectors. Each Jacobian element is then found through the forward difference before and after perturbation.

Damping Factor

Ideally, the damping factor is calculated such that the step is taken within an approximately linear region of the solution space. *Marquardt* (1963), suggested assuming an initial $\gamma = \gamma_0$, calculating a step, and performing the iteration. If the residual is increased, the step is rejected and γ is increased by a factor of ν. This is repeated until the step improves the residual and the iteration is kept. If the solution is improved sufficiently, γ can be reduced so the next iteration takes a larger step to decrease the number of iterations required for convergence. The difficulty in applying this technique to a coupled problem is that the residual for a particular altitude may increase due to coupling despite the solution moving closer to the true state. As well, calculating a damping factor based on the total residual may keep γ unnecessarily large for most altitudes, slowing convergence. This problem can be avoided by using a less rigorous determination of γ based on Marquardt's method, but with the relaxed constraint that the γ is only increased if the total residual increases past a certain point relative to the previous iteration. While this does not guarantee convergence, proper choice of this threshold can provide good results that are relatively robust and less affected by the altitude coupling. For this algorithm γ_0 is set to 0.02 and the iteration is kept provided the total residual does not increase by more than 2%.

Retrieval Steps

The coupled retrieval of aerosol number density and mode radius then proceeds as follows:

1. Determine the aerosol number density profile using the *a priori* particle size estimate and MART retrieval on the 750 nm measurement.
2. Calculate the Jacobian numerically based on the current estimate.
3. Determine the improved mode radius and extinction estimate at each altitude independently using the Levenberg-Marquardt algorithm.
4. a) If the increase in the total residual is more than 2% reset the atmospheric state to the previous iteration, set $\gamma = \gamma \cdot 10$ and proceed to step 2.
   b) If the total residual is reduced by more than a factor of five keep the step, set $\gamma = \gamma/2$ and proceed to step 2.
   c) If the solution has converged or the iteration limit has been reached, stop.
   d) Otherwise, proceed to step 2.

Iterations are stopped by testing for convergence or a maximum iteration limit. Convergence is checked by testing the flatness of the solution space at the current location through the norm of the Jacobian; whether progress is being made towards a solution through the step size; and whether the model has matched the measurements sufficiently. The convergence limits for the code tested here are given in Table 3.1, and are said to be satisfied if any of the limits are met for all retrieved altitudes.

Table 3.1: Levenberg Marquardt convergence limits

Jacobian Norm	Step Size	Total Residual	Iteration Limit
10^{-5}	0.01%	10^{-4}	20

Retrieved Parameters

The retrieved quantities of number density and mode radius are highly dependent on the microphysical assumptions in the model, namely that the aerosol distribution is a single mode lognormal with a mode width of 1.6. However, conversion of the retrieved parameters to more general quantities

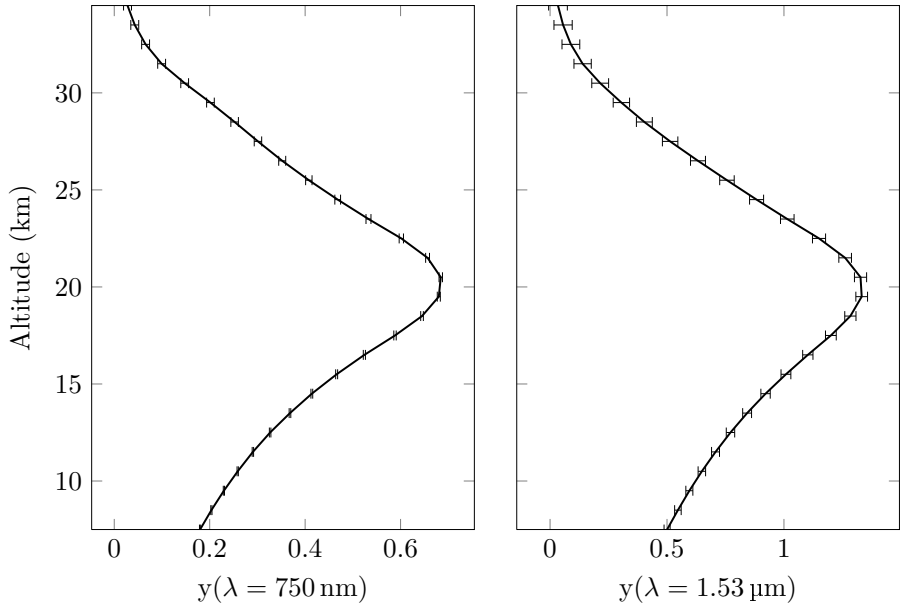

Figure 3.1: Measurement vectors shown with typical noise margins. Left panel is the 750 nm measurement and right panel is the 1.53 μm measurement.

can decrease this dependence. Extinction is much less dependent on the microphysical assumptions than number density (*McLinden et al.*, 1999) and is converted using the formula:

$$k_{\text{aer}}(\lambda) = n_{\text{aer}}\sigma_{\text{aer}}(\lambda), \tag{3.13}$$

where k_{aer} is the extinction and σ_{aer} the scattering cross section. Similarly, the mode radius is converted to an Ångström coefficient, α, using

$$\left(\frac{\lambda_1}{\lambda_2}\right)^{-\alpha} = \frac{\sigma_{\text{aer}}(\lambda_1)}{\sigma_{\text{aer}}(\lambda_2)}, \tag{3.14}$$

where λ_1 and λ_2 are the 750 nm and 1.53 μm wavelengths respectively.

3.2.4 Error Analysis

The following sections estimate the error of the retrieved quantities using the methods detailed by *Rodgers* (2000). Generally, the inverse problem is linearized about the retrieved atmospheric state with error calculations based on the sensitivity of the retrieved quantities to small perturbations in either the measurements or true atmospheric state. Calculations below consider only the uncorrelated errors.

3.2.4.1 Measurement Error

The uncorrelated error in the measurement vector y_k at altitude j can be determined from error in the radiance measurement as,

$$\delta y_{jk} = \frac{\delta I_j(\lambda_k)}{I_j(\lambda_k)}. \tag{3.15}$$

Typical measurement errors for a scan are shown in Figure 3.1. The covariance matrix of the measurement error, $\mathbf{S}_\epsilon$, is the diagonal matrix with elements δy_i^2. Propagation of this error through the

forward model is determined from the sensitivity of the retrieved quantity, $\hat{\mathbf{x}}$, to the measurement, $\mathbf{y}$, also known as the gain matrix, $\mathbf{G}$,

$$\mathbf{G} = \frac{\partial \tilde{\mathbf{x}}}{\partial \mathbf{y}}. \tag{3.16}$$

The covariance matrix of the retrieved quantity is then,

$$\mathbf{S}_m = \mathbf{G}\mathbf{S}_\epsilon\mathbf{G}^{\mathrm{T}}, \tag{3.17}$$

with the square root of the diagonal elements yielding the uncorrelated errors for the retrieved quantities.

3.2.4.2 Smoothing Error

Smoothing error results from the fact that measurements are not of a single point, but smoothed by an averaging kernel. Fluctuations in the true state with a higher resolution than the averaging kernel are thus undetectable, or largely so, and contribute to measurement error. This can be seen from computation of the averaging kernel, $\mathbf{A}$, which determines the change in the retrieved state, $\hat{\mathbf{x}}$, for a change in the true state, $\mathbf{x}$, or

$$\mathbf{A} = \frac{\partial \hat{\mathbf{x}}}{\partial \mathbf{x}}. \tag{3.18}$$

The magnitude of the smoothing error, $\boldsymbol{\epsilon}_s$, is then

$$\boldsymbol{\epsilon}_s = (\mathbf{A} - \mathbf{I})(\mathbf{x} - \mathbf{x}_a). \tag{3.19}$$

The uncorrelated smoothing error is calculated as the diagonal elements of $(\mathbf{A} - \mathbf{I})$ multiplied by the difference between the *a priori* and retrieved states, $(\mathbf{x} - \mathbf{x}_a)$.

3.2.4.3 Albedo Error

The albedo retrieval works well at 750 nm, however cannot be extended to the infrared imager due to lack of an absolute calibration. The current solution is the assumption that albedo is unchanged from 750 nm to 1.53 μm. While this assumption is certainly incorrect to some degree it is further complicated by the presence of a water vapor absorption band at 1.44 μm which extends slightly into the 1.53 μm detector's range. At stratospheric altitudes the water vapor mixing ratio is small, approximately 5 ppm (*Chiou et al.*, 1997), limiting the error in radiance to considerably less than that of measurement noise. At low altitudes however, water vapor can compose a substantial portion of the atmosphere, on the order of 1%, and ignoring water vapor is no longer valid. While retrievals are not performed at these low altitudes upwelling radiation in the water absorption bands will be systematically reduced, causing a reduction in the apparent albedo when compared to wavelengths outside of the absorption band. This likely leads to a systematic overestimation of the 1.53 μm albedo, although the amount will vary depending on atmospheric and ground conditions.

The magnitude of this error on the retrieved parameters can be determined in a similar fashion to the other error quantities through the formula

$$\boldsymbol{\epsilon}_b = \mathbf{G}\mathbf{K}_b(\mathbf{b} - \hat{\mathbf{b}}). \tag{3.20}$$

However, unlike measurement noise and smoothing errors, the error in albedo may be large, and the assumption that the forward model remains linear in the region of interest may be violated. A more accurate estimate of the error can be obtained by simulating retrievals with incorrect albedo values. Figure 3.2 shows the retrieved extinction and mode radius values for three cases where the true 1.53 μm albedo is 0.0, 0.5 and 1.0, while the assumed albedo is constant at 0.5. Both the true and assumed albedos for the 750 nm measurements are constant at 0.5 as well. The geometry of this scan was chosen to have a zenith angle of 72° and a scattering angle of 119° creating a relatively large

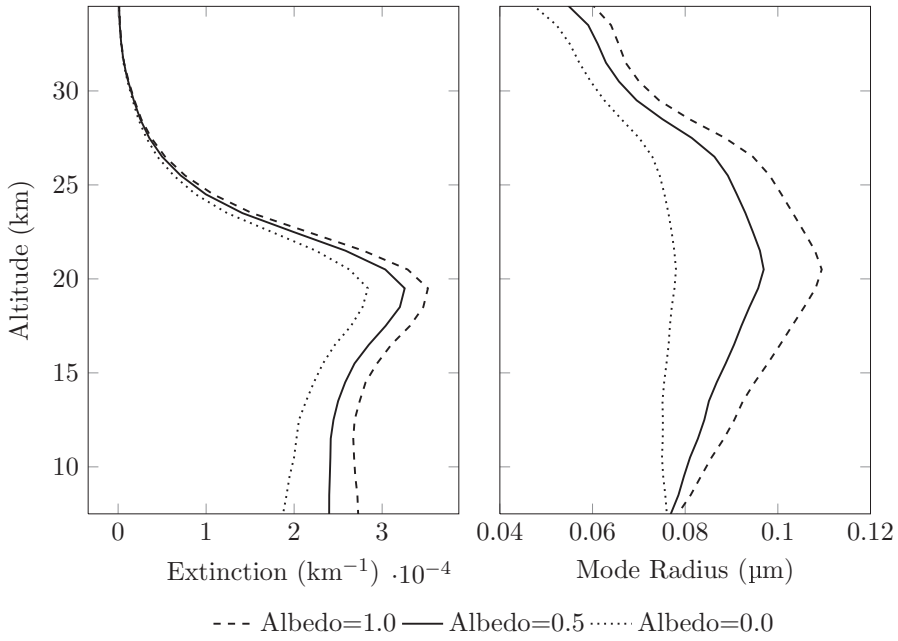

Figure 3.2: Error in the retrieval due to assumption that albedo is constant with wavelength.

albedo contribution to the total signal. If the true albedo is underestimated the measurement vector is systematically too large, leading to an increase of both particle size and extinction. For the geometry and cases tested the error due to incorrect albedo is approximately 15% for extinction and 30% for mode radius near the peak aerosol concentrations. The affect is also non-linear, with underestimation causing a larger error in both retrieved extinction and mode radius than overestimation. Note that this is close to a worst case, with albedo error of forward geometries for the same atmospheric conditions limited to less than 5% for both parameters.

The total error due these factors is summarized in Figure 3.3 as a percent of the true values for a strongly forward scatter geometry. At altitudes above 30 km and below 15 km error begins to dominate the signal, with virtually all of the error due to measurement noise. This is primarily due to the large error on the 1.53 μm measurements, which is approximately 5-10 times that of the 750 nm measurements.

3.2.4.4 Particle Size Error

Error due to incorrect particle size assumptions can be tested through simulated measurements and retrievals. The simulated atmosphere was assumed to be largely bimodal at lower altitudes, with coarse particles contributing approximately 50% of the overall extinction. The coarse mode fraction was decreased with altitude to simulate the sedimentation of larger particles, leading to an extinction due almost entirely to fine particles by 30 km. The fine mode parameters were also assumed incorrectly for the retrievals, with exact parameters given in Table 3.2. The simulated retrieval was tested with these atmospheric conditions for several hundred OSIRIS measurement geometries with results shown in Figure 3.4. The extinction and particle size retrieval has an error typically less than 10%, even when the true state is largely bimodal. The error in the retrieved Ångström coefficient is slightly larger, particularly at altitudes which are largely bimodal, however it still provides a large improvement over the *a priori* estimate.

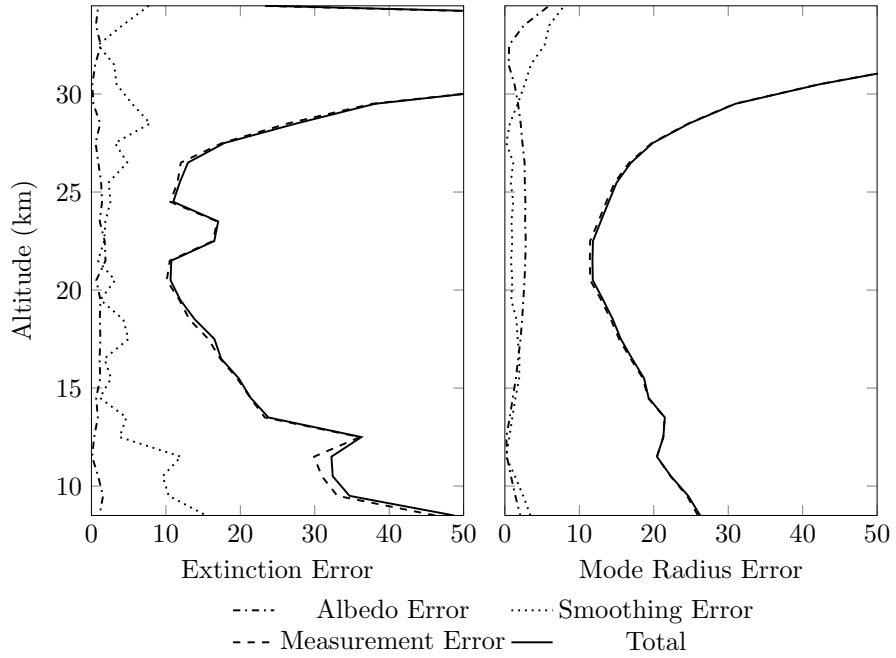

Figure 3.3: Total error in the retrieved quantities due to albedo, smoothing and measurement error contributions.

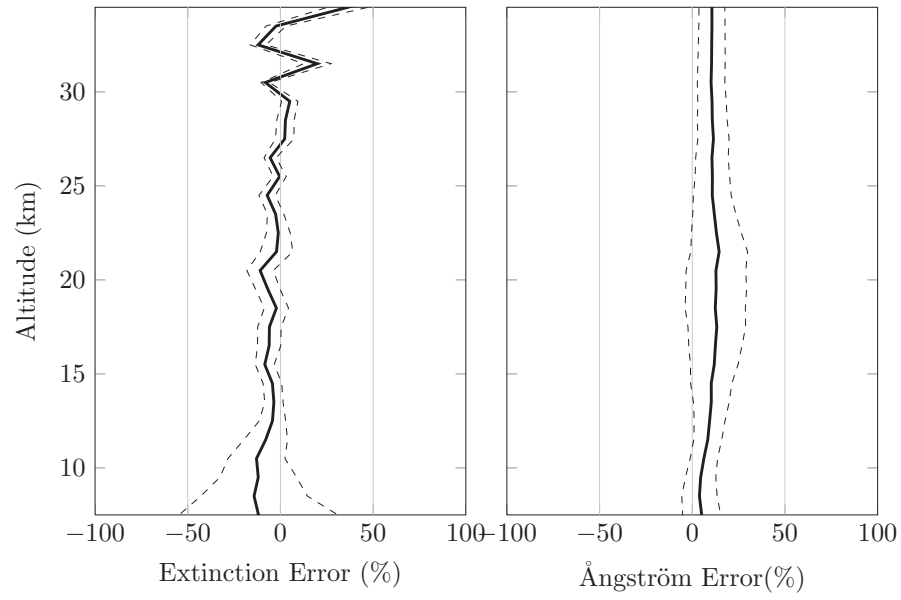

Figure 3.4: Error in the retrieved parameters under a variety of simulated measurement conditions when the true atmospheric state is bimodal. Percent error is shown as solid black line with standard deviation shown as dashed lines.

Table 3.2: Lognormal size parameters used in the simulated retrievals

Mode	MART Retrieval	Coupled Retrieval	True State
Fine Mode	$r_g = 80\,\text{nm}$ $\sigma_g = 1.60$	$r_g = N/A$ $\sigma_g = 1.60$	$r_g = 90\,\text{nm}$ $\sigma_g = 1.75$
Coarse Mode	$r_g = N/A$ $\sigma_g = N/A$	$r_g = N/A$ $\sigma_g = N/A$	$r_g = 400\,\text{nm}$ $\sigma_g = 1.20$

Bibliography

Bourassa, A. E., D. A. Degenstein, R. L. Gattinger, and E. J. Llewellyn (2007), Stratospheric aerosol retrieval with optical spectrograph and infrared imaging system limb scatter measurements, *J. Geophys. Res.*, *112*, D10,217, doi:10.1029/2006JD008079.

Bourassa, A. E., D. A. Degenstein, and E. J. Llewellyn (2008), SASKTRAN: A spherical geometry radiative transfer code for efficient estimation of limb scattered sunlight, *J. Quant. Spec. Radiat. Transf.*, *109*, 52–73, doi:10.1016/j.jqsrt.2007.07.007.

Bourassa, A. E., L. A. Rieger, N. D. Lloyd, and D. A. Degenstein (2011), Odin-OSIRIS stratospheric aerosol data product and SAGE III intercomparison, *Atmos. Chem. Phys. Discuss.*, *11*, 25,785–25,811, doi:10.5194/acpd-11-25785-2011.

Chahine, M. I. (1972), A General Relaxation Method for Inverse Solution of the Full Radiative Transfer Equation., *J. Atmos. Sci*, *29*, 741–747, doi:10.1175/1520-0469(1972)029$\langle$0741:AGRMFI$\rangle$2.0.CO;2.

Chahine, M. T. (1970), Inverse Problems in Radiative Transfer: Determination of Atmospheric Parameters., *J. Atmos. Sci.*, *27*, 960–967, doi:10.1175/1520-0469(1970)027$\langle$0960:IPIRTD$\rangle$2.0.CO;2.

Chiou, E. W., M. P. McCormick, and W. P. Chu (1997), Global water vapor distributions in the stratosphere and upper troposphere derived from 5.5 years of SAGE II observations (1986-1991), *J. Geophys. Res.*, *102*, 19,105–19,118, doi:10.1029/97JD01371.

Deshler, T., M. E. Hervig, D. J. Hofmann, J. M. Rosen, and J. B. Liley (2003), Thirty years of in situ stratospheric aerosol size distribution measurements from Laramie, Wyoming (41°N), using balloon-borne instruments, *J. Geophys. Res.*, *108*, 4167, doi:10.1029/2002JD002514.

Llewellyn, E., N. D. Lloyd, D. A. Degenstein, R. L. Gattinger, S. V. Petelina, A. E. Bourassa, J. T. Wiensz, E. V. Ivanov, I. C. McDade, B. H. Solheim, J. C. McConnell, C. S. Haley, C. von Savigny, C. E. Sioris, C. A. McLinden, E. Griffioen, J. Kaminski, W. F. J. Evans, E. Puckrin, K. Strong, V. Wehrle, R. H. Hum, D. J. W. Kendall, J. Matsushita, D. P. Murtagh, S. Brohede, J. Stegman, G. Witt, G. Barnes, W. F. Payne, L. Piche, K. Smith, G. Warshaw, D. L. Deslauniers, P. Marchand, E. H. Richardson, R. A. King, I. Wevers, W. McCreath, E. Kyrola, L. Oikarinen, G. W. Leppelmeier, H. Auvinen, G. Megie, A. Hauchecorne, F. Lefevre, J. de La Noe, P. Ricaud, U. Frisk, F. Sjoberg, F. von Scheele, and L. Nordh (2004), The OSIRIS instrument on the odin spacecraft, *Can. J. Phys.*, *82*, 411–422, doi:10.1139/p04-005.

Lloyd, N. D., and E. J. Llewellyn (1989), Deconvolution of blurred images using photon counting statistics and maximum probability, *Can. J. Phys.*, *67*, 89–+.

Marquardt, D. W. (1963), An algorithm for least-squares estimation of nonlinear parameters, *J. Soc. Ind. Appl. Math.*, *11*, pp. 431–441.

McLinden, C. A., J. C. McConnell, C. T. McElroy, and E. Griffioen (1999), Observations of Stratospheric Aerosol Using CPFM Polarized Limb Radiances., *J. Atmos. Sci.*, *56*, 233–240, doi: 10.1175/1520-0469(1999)056$\langle$0233:OOSAUC$\rangle$2.0.CO;2.

Rodgers, C. D. (2000), *Inverse methods for atmospheric sounding: theory and practice*, World Scientific.

von Savigny, C., C. S. Haley, C. E. Sioris, I. C. McDade, E. J. Llewellyn, D. Degenstein, W. F. J. Evans, R. L. Gattinger, E. Griffioen, E. Kyrölä, N. D. Lloyd, J. C. McConnell, C. A. McLinden, G. Mégie, D. P. Murtagh, B. Solheim, and K. Strong (2003), Stratospheric ozone profiles retrieved from limb scattered sunlight radiance spectra measured by the OSIRIS instrument on the Odin satellite, *Geophys. Res. Lett.*, *30*, 1755, doi:10.1029/2002GL016401.

3.3 Algorithms for Merging GOMOS and SAGE Aerosol Records (WP–26)

4 Algorithm Theoretical Baseline – Temperature

4.1 Algorithms for the Computation of Temperature Climatologies (WP–18)

Monthly mean zonal mean temperature climatologies were produced for ACE-FTS, MIPAS, and SMR following the same procedure as outlined in section 7.1 for short-lived species, in order to produce datasets on a common grid compatible the SPARC data initiative.

Monthly mean zonal mean temperature climatologies based on radio occultation (RO) data were produced as follows. CHAMP and GRACE data were obtained directly from the GFZ Helmholtz Centre in Potsdam (contacts: Jens Wickert and Torsten Schmidt). The source data consist of files of individual temperature profiles. Linear interpolation in log pressure coordinates was used to interpolate temperatures onto the pressure grid 300, 250, 200, 170, 150, 130, 115, 100, 90, 80, 70, 50, 30, 20, 15, 10, 7, 5, 3, 2, 1.5, and 1 hPa. Values at pressures below the bottom of the profile, or above the top of the profile, were omitted. Input data were also screened such that temperatures below 150 K were omitted as were temperatures above 330 K. The interpolated values were corrected for their zonal representativeness using NCEP (National Centers for Environmental Prediction) CFSR (Climate Forecast System Reanalyses) 6 hourly temperature fields on pressure surfaces as:

$$T_{corr} = T_{RO}(\theta, \phi, P, t) \times \frac{\overline{T_{CFSR}}(5^\circ, P, \text{month})}{T_{CFSR}(\theta, \phi, P, t)} \tag{4.1}$$

where

T_{corr} is the bias corrected temperature value,

T_{RO} is the radio occultation temperature measurement interpolated onto pressure P at latitude θ, longitude ϕ at time t,

$\overline{T_{CFSR}}(5^\circ, P, \text{month})$ is the NCEP-CFSR 5° zonal mean monthly mean temperature at pressure P, and

T_{CFSR} is the NCEP-CFSR temperature at the same time and location as T_{RO}.

Applying equation (4.1) corrects the radio occultation measurements for their sampling bias both in terms of geographical coverage and coverage within the month of interest. T_{corr} values were then accumulated into 5° latitude zones and monthly blocks. Averages of the data within each block were then calculated. These monthly means, together with the number of values used in each mean, are listed in the 36 (one for each 5° zone) output data files.

4.2 Algorithms for the Extension of the Upper Stratosphere Temperature Record (WP–23)

4.3 Algorithms for the Extension of the UT/LS Stratosphere Temperature Record (WP–24)

5 Algorithm Theoretical Baseline – Ozone

5.1 Algorithms for the GOMOS Bright Limb Ozone Analysis and Sample Processing (WP–17)

5.1.1 GOMOS bright limb processing

GOMOS (Global Ozone Monitoring by Occultation of Stars) is a spectrometer on board the European Space Agency's Envisat satellite (see Ref. Bertaux et al. (1991, 2000, 2004); Kyrölä et al. (2004); Bertaux et al. (2010); ESA (2001), and http://envisat.esa.int/dataproducts/gomos).

GOMOS is a medium resolution spectrometer. Spectrometers A1 and A2 cover the UV-visible wavelength region 248–690 nm with 1416 pixels with the spectral width 0.31 nm. The spectral resolution is 0.8 nm. The spectrometer B1 covers 755–774 nm with 420 0.045 nm wide pixels. The spectral resolution is 0.13 nm. The spectrometers B2 covers 926–954 nm with 500 0.052 nm wide pixels. The spectral resolution is 0.13 nm. The two photometers work at blue 473–527 nm and red 646–698 nm wavelengths at a frequency of 1 kHz (see Popescu and Paulsen (1999a)).

The ozone profiles obtained from the night time occultations are considered to have better than 5% accuracy at the stratosphere (van Gijsel et al., 2010; Renard et al., 2008; Meijer et al., 2004). However, the majority of the day time ozone profiles retrieved from occultations are currently of poor quality.

The GOMOS level 1b and Level 2 algorithms have been explained in Bertaux (1999); Kyrölä (1999); Kyrölä et al. (2010); Bertaux et al. (2010)). GOMOS error characterization have been discussed in Tamminen et al. (2010). GOMOS data products are discussed in Ref. Popescu and Paulsen (1999b).

In addition to the star signal, GOMOS also records the limb scattered sunlight during day time. The first experiment to retrieve ozone profiles from the limb signal was done by Taha et al. (2008). The processing presented here is based on Tukiainen et al. (2010).

5.1.2 GOMOS radiance measurements

GOMOS measures the atmosphere using three separate optical bands. The central band measures the sum of the star and the limb scattered signal, while the upper and the lower bands measure only the limb contribution. In the operational occultation retrieval, the upper/lower band radiance is removed from the central band measurement to get pure star signal, which is then used for the retrievals. This subtraction is performed for day and twilight observations but not in dark limb conditions (when the limb contribution is zero anyway).

5.1.2.1 Stray light removal

The GOMOS radiances suffer from severe stray light contamination at high tangent altitudes. The GOMOS stray light is a function of wavelength and altitude but the altitude dependence is complex and hard to model. The altitude dependence of stray light is affected by the cloud coverage below the satellite and the tangent point. There are several possible strategies to model the stray light. For the GOMOS bright limb v1.1 data we have used the simplest possible stray light estimator. We assume a constant stray light with only a spectral dependence (no altitude dependence). The stray light spectrum is calculated for each scan as a simple average

$$S(\lambda) = \frac{1}{N} \sum_{i=1}^{N} I(\lambda, i) \tag{5.1}$$

where i denotes tangent heights >100km. This constant stray light spectrum is subtracted from each altitude (radiance).

5.1.3 Inversion Method

For every measurement layer j, a least squares fit weighted by the standard deviation of the noise term is done between the model and measurement

$$\frac{\mathbf{I}(\mathrm{j},\lambda)}{\mathbf{I}_{\mathrm{ref}}(\lambda)} = \frac{\hat{\mathbf{I}}_{\mathrm{ss}}(\mathrm{j},\lambda,\rho)}{\hat{\mathbf{I}}_{\mathrm{ref}}(\lambda)}\mathbf{R} + \epsilon, \tag{5.2}$$

where $\mathbf{I}(\mathrm{j},\lambda)$ is the observed radiance and $\mathbf{I}_{\mathrm{ref}}(\lambda)$ is a reference measurement at ∼46 km. On the right hand side, $\hat{\mathbf{I}}_{\mathrm{ss}}(\mathrm{j},\lambda,\rho)$ is modeled single scattering radiance, adjusted dynamically during the fitting operations, and $\hat{\mathbf{I}}_{\mathrm{ref}}(\lambda)$ is modeled reference radiance. The second term on the right

$$\mathbf{R} = \frac{\hat{\mathbf{I}}_{\mathrm{tot}}(\mathrm{j},\lambda)}{\hat{\mathbf{I}}_{\mathrm{ss}}(\mathrm{j},\lambda)} \tag{5.3}$$

is the ratio of modeled total to single scattering radiance. This term comes from a look-up table calculated in advance with the Monte Carlo radiative transfer model Siro (Oikarinen et al., 1999). The modeled reference radiance is calculated

$$\hat{\mathbf{I}}_{\mathrm{ref}}(\lambda) = \hat{\mathbf{I}}_{\mathrm{ss}}(\lambda,\rho_{\mathrm{ecmwf}})\mathbf{R}_{\mathrm{ref}}, \tag{5.4}$$

where ρ_{ecmwf} are trace gas profiles taken from ECMWF data (air, temperature) and climatologies (O_3, NO_2, aerosols). The iterative fitting of gas densities ρ in Eq. (5.2) is done using the Levenberg-Marquardt method (Levenberg, 1944; Marquardt, 1963) minimizing the chi square function

$$\chi^2 = (\mathbf{T}_{\mathrm{obs}} - \mathbf{T}_{\mathrm{mod}})^{\mathrm{T}}\mathbf{C}^{-1}(\mathbf{T}_{\mathrm{obs}} - \mathbf{T}_{\mathrm{mod}}), \tag{5.5}$$

where $\mathbf{T}_{\mathrm{obs}}$ and $\mathbf{T}_{\mathrm{mod}}$ denote ratios of Eq. (5.2) and $\mathbf{C}$ is the diagonal error covariance matrix including variance of the measurement (ratio) error. The standard deviation of the radiance $\mathbf{I}(\mathrm{j},\lambda)$ is approximated as

$$\sigma_{\mathrm{rad}}(\mathrm{j},\lambda) = \sqrt{\mathbf{I}_{\mathrm{e}}(\mathrm{j},\lambda) + \mathbf{I}_{\mathrm{sc}}(\lambda) + \mathbf{I}_{\mathrm{dc}}(\lambda)}\mathbf{Z}(\lambda), \tag{5.6}$$

where $\mathbf{I}_{\mathrm{e}}(\mathrm{j},\lambda)$ is the uncorrected radiance as electrons, $\mathbf{I}_{\mathrm{sc}}(\lambda)$ is the approximate variance of the stray light estimate, $\mathbf{I}_{\mathrm{dc}}(\lambda)$ is the contribution from the dark charge, and $\mathbf{Z}(\lambda)$ is the radiometric sensitivity curve to convert the values into physical units. The variance of the radiance ratio $\frac{\mathbf{I}(\mathrm{j},\lambda)}{\mathbf{I}_{\mathrm{ref}}(\lambda)}$ is approximated as

$$\sigma^2_{\mathrm{ratio}}(\mathrm{j},\lambda) = (\frac{\sigma_{\mathrm{rad}}(\mathrm{j},\lambda)}{\mathbf{I}_{\mathrm{ref}}(\lambda)})^2 + (\frac{\mathbf{R}(\mathrm{j},\lambda)\sigma_{\mathrm{rad}}(\mathrm{j}_{\mathrm{ref}},\lambda)}{\mathbf{I}_{\mathrm{ref}}(\lambda)})^2, \tag{5.7}$$

where $\mathbf{I}_{\mathrm{ref}}(\lambda)$ is the measurement reference radiance, $\mathbf{R}(\mathrm{j},\lambda)$ is the modeled tot/ss ratio, and $\sigma_{\mathrm{rad}}(\mathrm{j}_{\mathrm{ref}},\lambda)$ is the standard deviation of the radiance at the reference altitude. Currently, no modeling error is added in the covariance matrix $\mathbf{C}$.

The atmosphere between around 60 and 20 km is "peeled" this way from top to down to get the vertical profiles of retrieved species. We retrieve O_3, aerosols and neutral air together while NO_2 is taken from a climatology and kept fixed.

5.1.3.1 Processing

The schematic presentation of the processing chain is shown in Fig. 5.2

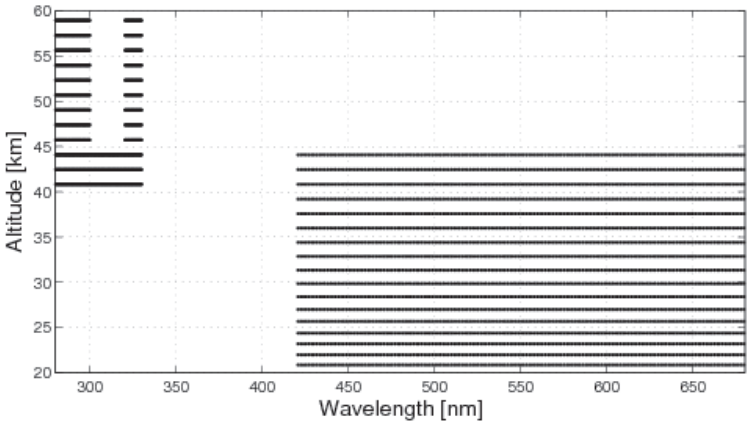

Figure 5.1: GOMOS wavelengths used in the bright limb ozone retrieval.

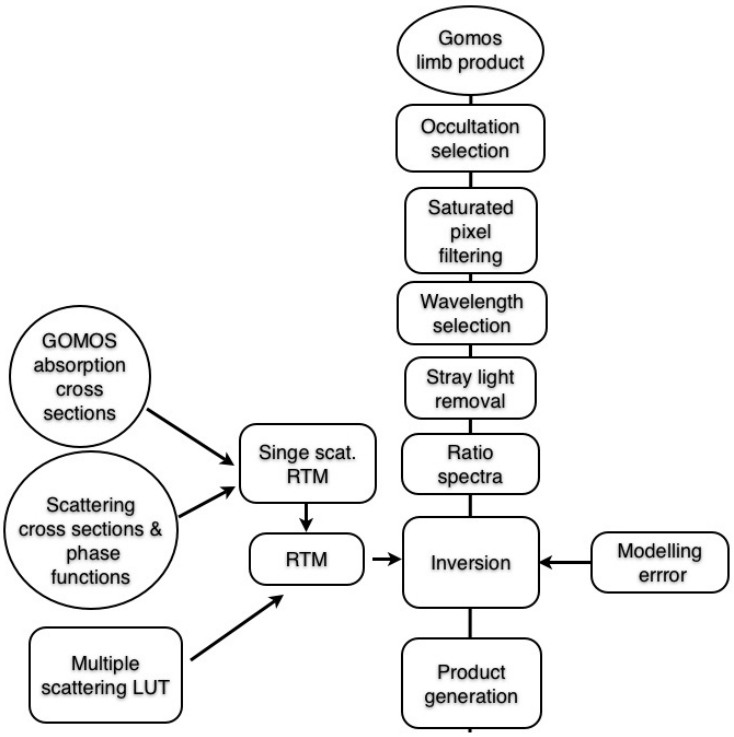

Figure 5.2: GOMOS bright limb processing

Bibliography

J. L. Bertaux. GOMOS ATBD—Level 1b. In *ESAMS99, European Symposium on Atmospheric Measurements From Space*, volume WPP-161, pages 115–123, Noordwijk, 1999. ESA.

J. L. Bertaux, G. Megie, T. Widemann, E. Chassefiere, R. Pellinen, E. Kyrölä, S. Korpela, and P. Simon. Monitoring of ozone trend by stellar occultations: The GOMOS instrument. *Adv. Space Res.*, 11(3):237–242, 1991.

J. L. Bertaux, E. Kyrölä, and T. Wehr. Stellar occultation technique for atmospheric ozone monitoring: GOMOS on Envisat. *Earth Observation Quarterly*, 67:17–20, 2000.

J. L. Bertaux, A. Hauchecorne, F. Dalaudier, C. Cot, E. Kyrölä, D. Fussen, J. Tamminen, G. W. Leppelmeier, V. Sofieva, S. Hassinen, O. Fanton d'Andon, G. Barrot, A. Mangin, B. Théodore, M. Guirlet, O. Korablev, P. Snoeij, R. Koopman, and R. Fraisse. First results on GOMOS/Envisat. *Adv. Space Res.*, 33:1029–1035, 2004.

J. L. Bertaux, E. Kyrölä, D. Fussen, A. Hauchecorne, F. Dalaudier, V. Sofieva, J. Tamminen, F. Vanhellemont, O. Fanton D'Andon, G. Barrot, A. Mangin, L. Blanot, J. C. Lebrun, K. Pérot, T. Fehr, L. Saavedra, G. W. Leppelmeier, and R. Fraisse. Global ozone monitoring by occultation of stars: an overview of GOMOS measurements on ENVISAT. *Atmospheric Chemistry & Physics*, 10:12091–12148, December 2010. doi: 10.5194/acp-10-12091-2010.

ESA. *Envisat-GOMOS, An instrument for global atmospheric ozone monitoring*, volume SP-1244. European Space Agency, 2001.

E. Kyrölä. GOMOS ATBD—Level 2. In *ESAMS99, European Symposium on Atmospheric Measurements From Space*, volume WPP-161, pages 125–137, Noordwijk, 1999. ESA.

E. Kyrölä, J. Tamminen, G. W. Leppelmeier, V. Sofieva, S. Hassinen, J.-L. Bertaux, A. Hauchecorne, F. Dalaudier, C. Cot, O. Korablev, O. Fanton d'Andon, G. Barrot, A. Mangin, B. Theodore, M. Guirlet, F. Etanchaud, P. Snoeij, R. Koopman, L. Saavedra, R. Fraisse, D. Fussen, and F. Vanhellemont. GOMOS on Envisat: An overview. *Adv. Space Res.*, 33:1020–1028, 2004.

E. Kyrölä, J. Tamminen, V. Sofieva, J. L. Bertaux, A. Hauchecorne, F. Dalaudier, D. Fussen, F. Vanhellemont, O. Fanton D'Andon, G. Barrot, M. Guirlet, A. Mangin, L. Blanot, T. Fehr, L. Saavedra de Miguel, and R. Fraisse. Retrieval of atmospheric parameters from GOMOS data. *Atmospheric Chemistry & Physics*, 10:11881–11903, December 2010. doi: 10.5194/acp-10-11881-2010.

K. Levenberg. A method for the solution of certain problems in least squares. *Quart. Appl. Math.*, 2:164–168, 1944.

D.W Marquardt. An Algorithm for Least-Squares Estimation of Nonlinear Parameters. *J. Soc. Indust. Appl. Math.*, 11:431–44, 1963.

Y. J. Meijer, D. P. J. Swart, M. Allaart, S. B. Andersen, G. Bodeker, Boyd, G. Braathena, Y. Calisesia, H. Claude, V. Dorokhov, P. von der Gathen, M. Gil, S. Godin-Beekmann, F. Goutail, G. Hansen, A. Karpetchko, P. Keckhut, H. M. Kelder, R. Koelemeijer, B. Kois, R. M. Koopman, J.-C. Lambert, T. Leblanc, I. S. McDermid, S. Pal, G. Kopp, H. Schets, R. Stubi, T. Suortti, G. Visconti, , and M. Yela. Pole-to-pole validation of ENVISAT/GOMOS ozone profiles using data from ground-based and balloon-sonde measurements. *J. Geophys. Res.*, 109(D23):art. no D23305, 2004. doi: 10.1029/2004JD004834.

L. Oikarinen, E. Sihvola, and E. Kyrölä. Multiple scattering radiance in limb-viewing geometry. *J. Geophys. Res.*, 104(D24):31,261–31,274, 1999.

A. Popescu and T. Paulsen. Gomos instrument on Envisat. In *ESAMS99, European Symposium on Atmospheric Measurements from Space*, volume WPP-161, pages 89–99. ESA, 1999a.

A. Popescu and T. Paulsen. Gomos data products. In *ESAMS99, European Symposium on Atmospheric Measurements from Space*, volume WPP-161, pages 111–114. ESA, 1999b.

J.-B. Renard, G. Berthet, C. Brogniez, V. Catoire, D. Fussen, F. Goutail, H. Oelhaf, J.-P. Pommereau, H. K. Roscoe, G. Wetzel, M. Chartier, C. Robert, J.-Y. Balois, C. Verwaerde, F. Auriol, P. François, B. Gaubicher, and P. Wursteisen. Validation of GOMOS-Envisat vertical profiles of O_3, NO_2, NO_3, and aerosol extinction using balloon-borne instruments and analysis of the retrievals. *Journal of Geophysical Research (Space Physics)*, 113(A12):A02302, February 2008. doi: 10.1029/2007JA012345.

G. Taha, G. Jaross, D. Fussen, F. Vanhellemont, E. Kyrölä, and R. D. McPeters. Ozone profile retrieval from GOMOS limb scattering measurements. *Journal of Geophysical Research (Atmospheres)*, 113(D12):23307–+, December 2008. doi: 10.1029/2007JD009409.

J. Tamminen, E. Kyrölä, V. F. Sofieva, M. Laine, J.-L. Bertaux, A. Hauchecorne, F. Dalaudier, D. Fussen, F. Vanhellemont, O. Fanton-D'Andon, G. Barrot, A. Mangin, M. Guirlet, L. Blanot, T. Fehr, L. Saavedra de Miguel, and R. Fraisse. GOMOS data characterisation and error estimation. *Atmospheric Chemistry & Physics*, 10:9505–9519, October 2010. doi: 10.5194/acp-10-9505-2010.

S. Tukiainen, S. Hassinen, A. Seppälä, H. Auvinen, E. Kyrölä, J. Tamminen, C. S. Haley, N. Lloyd, and P. T. Verronen. Description and validation of a limb scatter retrieval method for Odin/OSIRIS. *Journal of Geophysical Research (Atmospheres)*, 113(D12):4308–+, February 2008. doi: 10.1029/2007JD008591.

S. Tukiainen, E. Kyrölä, P. T. Verronen, D. Fussen, L. Blanot, G. Barrot, A. Hauchecorne, and N. Lloyd. Retrieval of ozone profiles from GOMOS limb scattered measurements. *Atmospheric Measurement Techniques Discussions*, 3:4355–4382, October 2010. doi: 10.5194/amtd-3-4355-2010.

J. A. E. van Gijsel, D. P. J. Swart, J.-L. Baray, H. Bencherif, H. Claude, T. Fehr, S. Godin-Beekmann, G. H. Hansen, P. Keckhut, T. Leblanc, I. S. McDermid, Y. J. Meijer, H. Nakane, E. J. Quel, K. Stebel, W. Steinbrecht, K. B. Strawbridge, B. I. Tatarov, and E. A. Wolfram. GOMOS ozone profile validation using ground-based and balloon sonde measurements. *Atmospheric Chemistry & Physics Discussions*, 10:8515–8551, 2010.

5.2 Algorithms for Merging Vertical Ozone Profile Measurements (WP–22)

6 Algorithm Theoretical Baseline – Water Vapor

6.1 Algorithms for the Maturation of SCIAMACHY Water Vapor Products (WP–13)

The current version of the water vapor retrieval (V3.01) from SCIAMACHY limb measurements is largely identical with the version 3 presented in Rozanov et al. (2011). The IUP-scientific retrieval processor is based on the software package SCIATRAN (Rozanov et al., 2002) Version 3.1. The water vapor retrieval from SCIAMACHY limb measurements done using the Optimal Estimation type approach (Rodgers, 2000) with first order Tikhonov constraints. Neglecting all errors, the linearized inverse problem is written as

$$\vec{y} = \vec{F}\left(\vec{x}_{\mathtt{a}}\right) + \mathbf{K}\left(\vec{x} - \vec{x}_{\mathtt{a}}\right), \tag{6.1}$$

where the mapping $\vec{F}$ represents the radiative transfer operator, $\vec{y}$ is the measurement vector, $\vec{x}$ is the state vector with the atmospheric parameters,

$$\mathbf{K} \equiv \left.\frac{\partial \vec{F}(\vec{x})}{\partial \vec{x}}\right|_{\vec{x}\,=\,\vec{x}_{\mathtt{a}}} \tag{6.2}$$

is the Jacobian matrix or weighting function matrix.

The linear inverse ill-posed problem represented by Eq. 6.1 is solved minimizing:

$$\left\|\vec{F}\left(\vec{x}_{\mathtt{a}}\right) + \mathbf{K}\left(\vec{x} - \vec{x}_{\mathtt{a}}\right) - \vec{y}\right\|^2_{\mathbf{P}} + \left\|\left(\vec{x} - \vec{x}_{\mathtt{a}}\right)\right\|^2_{\mathbf{Q}} \longrightarrow \min. \tag{6.3}$$

Here, $\mathbf{Q}$ is a constraint matrix for the state vector and $\mathbf{P} = \mathbf{S}_{\varepsilon}^{-1}$ is the inverse error covariance matrix of the measurement vector $\vec{y}$. The matrix $\mathbf{S}_{\varepsilon}$ is often referred to as the noise covariance matrix. The state vector constraint matrix, $\mathbf{Q}$, consist of two matrices, namely, the inverse a priori covariance matrix as commonly used in the optimal estimation approach (Rodgers, 2000) and a smoothness constraint matrix:

$$\mathbf{Q} = \mathbf{S}_{\mathtt{a}}^{-1} + \mathbf{R}^T\mathbf{R}. \tag{6.4}$$

The solution of the linear inverse problem given by Eq. (6.3) is obtained as follows:

$$\vec{x} = \vec{x}_{\mathtt{a}} + \Big(\mathbf{K}^T\,\mathbf{P}\,\mathbf{K} + \mathbf{Q}\Big)^{-1}\mathbf{K}^T\,\mathbf{P}\Big(\vec{y} - \vec{F}\left(\vec{x}_{\mathtt{a}}\right)\Big). \tag{6.5}$$

6.1.1 SCIAMACHY limb measurements and calibration

For the water vapor retrieval limb data from channel 6 between 1352 and 1410 nm are used. We use level 1c data version 7.03 (before 21 June 2010) and 7.04 afterward. There are two different consolidation versions for V 7.04: U and W. It was not possible to use a consistent level 1 version due to the long time necessary to process the water vapor retrieval. The influence of different level 1c data on the result were tested and are usually negligible. The spectral sampling is 0.78 nm, the spectral resolution 1.26 (FWHM) in this wavelength range. The following pixels numbers of channel 6 are excluded as bad or death pixels: 5405, 5630, 5631, 5787, 5788, 5803, 5804, and 5843. Spectra of tangent height number 6 to 10 (about 12.0, 15.3, 18.6, 21.9, 25.2 km) are used for the water vapor retrieval, i.e. the vertical sampling is about 3.3 km. The vertical instantaneous field of view of the

SCIAMACHY instrument is about 2.6 km at the tangent point, the horizontal cross-track resolution about 240 km (Rozanov et al., 2011). The spectra are calibrated for non-linearity, leakage current, pixel-to-pixel gain, stray light, and wavelength (calibration flags 0,1,2,4,5, etalon (3) does not apply for channel 6 data). No polarization correction and no absolute radiometric calibration are applied. For the limb dark correction the GADS (Global Annotation Dataset) correction is used. The limb spectra are divided by the uncalibrated ASM diffuser solar spectrum at each tangent height. For the retrieval, only the differential absorption structure is considered. This is calculated by subtracting a cubic polynomial from all measured limb and simulated spectra.

6.1.2 Auxiliary Data

The temperature and pressure profiles for the location, date and time of each limb measurement are taken from the ECMWF ERA-Interim reanalysis.

6.1.3 Cloud filter

Clouds can be identified in SCIAMACHY measurements through a color ratio method (see Savigny et al., 2005, Eichmann et al., 2009, and Rozanov et al., 2011). We use V1.9 of the cloud filter with three wavelength pairs ((750 nm, 1090 nm), (1090 nm, 1552 nm) and (1552 nm, 1685 nm)) and exclude all profiles, where clouds are detected higher than 10 km altitude.

6.1.4 Radiative transfer model

The spectra are simulated using the forward model of SCIATRAN. The single scattered contribution is calculated in a fully spherical atmosphere. The multiple scattered contribution is calculated with the combined differential-integral approach using a pseudo-spherical model with solar zenith angle and viewing angles set according to the spherical ray tracing. The refraction is taken into account during ray tracing. Weighting functions are calculated using the single scattering approximation. The forward model uses the correlated-k distribution technique (Buchwitz et al., 2000) with ESFT (exponential-sum fitting of transmissions) coefficients calculated using the HITRAN 2008 database (Rothman et al., 2009). This data set uses 10 coefficients precalculated at 20 pressure and 9 temperature grid points for 0.2 nm spectral bins. The SNR is calculated from the residuals of the spectra after the shift correction (see Sect. 6.1.5) with a correction factor of 1.5. The SNR is usually between 400 and 700 and increases from lower to higher altitudes.

6.1.5 Shift correction

All spectra are corrected for a possible wavelengths misalignment. The misalignment can be caused by a changing illumination of the instrument entrance slit during the vertical scan and temperature distension of the detector array. The correction is performed for each tangent height independently minimizing the following quadratic form with respect to parameters s_i, $c_{\rm sim}$, and $c_{\rm sol}$ The subscript n is omitted although s_i, $c_{\rm sim}$, and $c_{\rm sol}$ are tangent height dependent.

$$\left\| \hat{I}_{\rm n}(\lambda) - \hat{I}_{\rm sol}(\lambda) - \hat{I}_n^{\rm sim}(\lambda) - \sum_{i=1}^{5} s_i\, W_{{\rm n},i}(\lambda) - c_{\rm sim}\, \frac{\partial \hat{I}_{\rm n}^{\rm sim}(\lambda)}{\partial \lambda} - c_{\rm sol}\, \frac{\partial \hat{I}_{\rm sol}(\lambda)}{\partial \lambda} \right\|^2 \longrightarrow \text{min.} \quad (6.6)$$

Hence, $W_{n,i}(\lambda)$ are the vertically integrated weighting functions for water vapor and methane with $i = 1, 2$ and the weighting functions for albedo, tropospheric correction, and stratospheric aerosol extinction with $i = 3, 4, 5$. A spectral point is considered as an outlier if the remaining residual is larger than six times the RMS.

6.1.6 Iterative approach

A Gauss-Newton iterative scheme (Rodgers, 2000) is applied to account for the non-linearity of the inverse problem. For x_{i+1} Eq. 6.5 results in:

$$\vec{x}_{\mathtt{i+1}} = \vec{x}_{\mathtt{a}} + \left(\mathbf{K}_{\mathtt{i}}^T\ \mathbf{P}\ \mathbf{K}_{\mathtt{i}} + \mathbf{Q}\right)^{-1} \times \mathbf{K}_{\mathtt{i}}^T\,\mathbf{P}\Big(\vec{y} - \vec{F}\,(x_{\mathtt{i}})\ + \mathbf{K}_{\mathtt{i}}\,(\vec{x}_{\mathtt{i}} - \vec{x}_{\mathtt{a}})\Big). \quad (6.7)$$

The iterative process, which is limited to a maximum of 12 steps, is stopped after one of the following convergence criteria is reached. The first criterion is that the relative change of the root mean square (RMS) of the fit residual $RMS_{i+1}/RMS_i - 1$ is lower than 10^{-3}. The second criterion is the relative change of the retrieved parameters with a threshold of 0.01%, which is defined as the maximum change in the number densities between 12 km and 23 km.

6.1.7 Methane

Absorption bands of methane are included in the retrieval. This improves the spectral fits, although the methane absorption is much weaker than the one for water vapor. Therefore, a reliable retrieval of methane is not possible.

6.1.8 Albedo

Because also the differential absorption structure is influenced by the albedo, it is included in the retrieval using the numerical perturbation method (with a perturbation of 0.3) to obtain weighting functions.

6.1.9 Tropospheric correction

The retrieval includes a tropospheric correction, i.e. the scaling of the tropospheric profile and surface elevation. In each iteration either the scaling factor for the tropospheric correction or the surface elevation is retrieved using the numerical perturbation method to obtain the corresponding weighting functions. The perturbation is 4 km in the first iteration and 2 km in all other iterations for the elevation. For the scaling of the tropospheric column the perturbation is -80%. The surface elevation is retrieved at least during the first 3 iterations. The retrieval of the scaling of the tropospheric profile is started, when the result for the surface elevation changed with less than 0.5 km between the two preceding iterations.

6.1.10 Aerosol correction

The stratospheric aerosols are assumed to be non-absorbing. The vertical profile of the aerosol extinction coefficient is estimated by fitting radiance profiles averaged around 1090 and 1552 nm. The LOWTRAN background aerosol (Kneizys et al., 1986) is used for the phase function and as a priori. For the troposphere, the retrieved aerosol extinction for the lowest altitude is maintained and the profile shape from the a priori profile is used employing a smoothing constraint of 10 km. In the water vapor retrieval a scaling factor for the aerosol profile is retrieved. The numerical perturbation method (with a perturbation of 0.5) is used to obtain weighting functions. Only altitudes higher than 10 km are perturbed to determine the scaling factor.

6.1.11 Regularization

The trace gas vertical distributions according to the US Standard 1976 model atmosphere are used as a priori for methane and water vapor. A priori uncertainties are set to 300% for water vapor, 30%

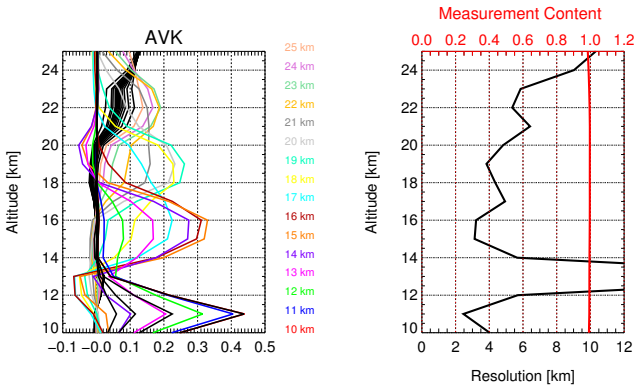

Figure 6.1: Averaging Kernels (left) and resolution (right) of a profile which is sorted out by the resolution filter.

for methane. Different to Rozanov et al. (2011) the a priori for tropospheric contribution, surface albedo and stratospheric aerosol scaling are not replaced after each iterative step to achieve a faster convergence. The a priori uncertainties are: 0.1 for albedo, 30% for stratospheric aerosol scaling, 100% for tropospheric scaling, and 3 km for elevation For water vapor, the smoothness coefficient increases linearly from 5 at 10 km to 10 at 30 km, while smoothness coefficient of 1 is used at all altitude layers for methane.

6.1.12 Data filtering

The retrieved profiles are filtered based on convergence of the retrieval and RMS of the residual. Tests with different filters were performed, resulting in two different data sets, V3.01 and V3.02. Before the retrieval is performed, V3.01 is filtered for clouds (see Subsect. 6.1.3) and data which could be influenced by the South Atlantic Anomaly (SAA). Additionally, all profiles were the retrieval is not converging within 12 iterations are omitted. This is slightly different to the water vapor data in SPARC (V3.0), where profiles are only omitted, if the retrieval does not reach convergence and the RMS of the residual is larger than 0.01. For V3.02 an additional filter for the resolution is applied. The resolution is calculated as inverse of the information content, which is given by the diagonal elements of the Averaging Kernel (AVK) matrix. In V3.02 profiles are excludes, if the resolution exceeds 8 km between 11 and 20 km altitude or if a resolution is smaller or equal to zero. This should exclude profiles, with reduced data quality in parts of the profile. An analysis of the filtered data shows that many profiles in the mid and high latitudes are filtered, where the vertical distance between the lowest measurements is increased due to refraction. If a retrieval grid point falls exactly between two measurement altitudes, this results in two maximums of the AVK and unrealistic resolution values. An example is shown in Fig. 6.1, where this occurs for 13 km height. In these cases, the resolution indicates that the retrieval grid is too dense compared to the vertical sampling. This means for the effected altitudes that they contain only information from above and below, but should not decrease the quality of the profile in general. Therefore it is questionable, if the resolution filter should be applied.

6.1.13 Error Characterization

The error characterization is expected to be similar to the one for V3 presented in Rozanov et al. (2011), which is based on simulated retrieval and is summarized below. An error characterization for data V3.01 remains still to be done. Albedo, a scaling factor for aerosols and surface elevation are part of the retrieval.

1. Albedo The effects of tropospheric albedo on the retrieval is smaller than 0.5 % if an albedo of 1 or 0 is assumed and the real albedo is 0.5.

2. Tropospheric water vapor A doubling/halving of the tropospheric water vapor causes errors up to about 3 %.

3. Aerosol Errors due to stratospheric aerosols are usually smaller than 10 %. An exception is high volcanic aerosol loading, but this does occur seldom during the measurement time of SCIAMACHY and should be excluded by the cloud filter.

4. Clouds Errors due to clouds below the retrieved profile are usually about 10 %, they can reach up to 20 % for large scattering angles.

5. Surface elevation Assuming a surface elevation of 6 km when it is 2.2 km leads to an error of up to 2 %.

Bibliography

Buchwitz, M., Rozanov, V. V., and Burrows, J. P.: A correlated-k distribution scheme for overlapping gases suitable for retrieval of atmospheric constituents from moderate resolution radiance measurements in the visible/near-infrared spectral region, J. Geophys. Res., 105, 15247–15261, 2000.

Eichmann, K.-U., von Savigny, C., Reichl, P., Robert, C., Steinwagner, J., Bovensmann, H., and Burrows, J. P.: SCODA: SCIAMACHY Cloud Detection Algorithm from Limb Radiance Measurements - Algorithm theoretical basis document, Tech. rep., Institute of Environmental Physics, University of Bremen, unpublished technical document, 2009.

Kneizys, F. X., Shettle, E. P., Abreu, L. W., Chetwynd, J. H., Anderson, G. P., Gallery, W. O., Selby, J. E. A., and Clough, S. A.: Users Guide to LOWTRAN 7, Tech. rep., Air Force Geophysics Laboratory AFGL, 1986.

Rodgers, C. D.: Inverse Methods for Atmospheric Sounding: Theory and Practice,World Scientific, 2000.

Rothman, L., Gordon, I., Barbe, A., Benner, D., Bernath, P., Birk, M., Boudon, V., Brown, L., Campargue, A., Champion, J.-P., Chance, K., Coudert, L., Dana, V., Devi, V., Fally, S., Flaud, J.-M., Gamache, R., Goldman, A., Jacquemart, D., Kleiner, I., Lacome, N., Lafferty, W., Mandin, J.-Y., Massie, S., Mikhailenko, S., Miller, C., Moazzen-Ahmadi, N., Naumenko, O., Nikitin, A., Orphal, J., Perevalov, V., Perrin, A., Predoi-Cross, A., Rinsland, C., Rotger, M., Simeckova, M., Smith, M., Sung, K., Tashkun, S., Tennyson, J., Toth, R., Vandaele, A., and Vander Auwera, J.: The HITRAN 2008 molecular spectroscopic database, J. Quant. Spectrosc. Ra., 110, 533–572, doi:10.1016/j.jqsrt.2009.02.013, 2009.

Rozanov, V. V., Buchwitz, M., Eichmann, K.-U., De Beek, R., and Burrows, J. P. SCIATRAN - a new radiative transfer model for geophysical applications in the 240 – 2400 nm spectral region: The pseude-spherical version. Adv. Space. Res. 29, 11, 1831 – 1835, 2002.

Rozanov, A., K. Weigel, H. Bovensmann, S. Dhomse, K.-U. Eichmann, R. Kivi, V. Rozanov, H. V?mel, M. Weber, and J. P. Burrows, Retrieval of water vapor vertical distributions in the upper troposphere and the lower stratosphere from SCIAMACHY limb measurements, Atmos. Meas. Techn., 4, 933-954, doi:10.5194/amt-4-933-2011, 2011

von Savigny, C., Ulasi, E. P., Eichmann, K.-U., Bovensmann, H., and Burrows, J. P.: Detection and mapping of polar stratospheric clouds using limb scattering observations, Atmos. Chem. Phys., 5, 3071-3079, doi:10.5194/acp-5-3071-2005, 2005.

6.2 Algorithms for Merging Vertical Water Vapor Profile Measurements (WP–27)

7 Algorithm Theoretical Baseline – Short Lived Species

In this section the theoretical baseline of the algorithms used for creating short-lived species climatologies is described. Section 7.1 summarises the general methodology adopted for creating climatologies (including short-lived species) within the SPARC data initiative. Further, we briefly outline in Section 7.2 the algorithms used for creating "scaled" climatologies with respect to local solar time.

7.1 Algorithms for the Computation of Short Lived Species Climatologies (WP–16)

The description below is based on a draft version of the SPARC data initiative (SPARC-DI) report. For instrument specific details please consult the report.

SPARC-DI monthly zonal mean trace gas climatologies are calculated for each species using 5∘ latitude bins on a pressure grid with 28 levels between 300 and 0.1 hPa. The original data products are first interpolated to the SPARC pressure grid using log-linear interpolation. For instruments providing data on an altitude grid conversion from altitude to pressure levels is done using retrieved temperature/pressure profiles or meteorological analyses. The same pressure and temperature profiles are used to convert products to volume mixing ratio if number densities are retrieved. Original data have been carefully screened according to recommendations given in relevant quality documents, in published literature, or according to best knowledge of the involved instrument scientists. Zonal mean products are calculated as the average of all of the measurements on a given pressure level within each latitude bin. For some species and instruments, averaging was done in log(VMR) (instead of VMR) space. Typically a minimum of 5 measurements within the bin is required. The mean value and the 1-σ standard deviation of the measurements, along with the number of averaged data values, are given within each latitude bin at each pressure level. The mean, minimum, and maximum local solar time, average day of the month, and average latitude of the data within each bin for a selected pressure level are also provided.

For species with large diurnal variations the measurements are separated based on the local solar time. Additional climatologies are built using a photochemical box model to scale the measurements to a common local solar time in order to enable direct comparison between products from different instruments with different sampling patterns.

7.2 Algorithms for Creating Local Time Corrected Climatologies (WP–16)

Most of the instruments measure at two distinct local solar times at each latitude, either because they are in polar sun-synchronous orbit, with one local solar time for the ascending orbit and one for the descending orbit, or because they are solar occultation instruments that measure only at sunrise and sunset as seen from the satellite. The climatologies for the instruments that sample two local solar times are separated into AM and PM. Instruments observing from non sun-synchronous orbits are characterised by drifting observation times with respect to local solar time. Climatologies for those instruments are roughly separated into daytime and nighttime measurements.

Scaled climatologies are calculated for 10 AM and 10 PM, the approximate local time of the Envisat/MIPAS measurements, for all short-lived species (e.g. NO, NO_2, etc.) with exception of ClO. The ClO climatologies are scaled to 1:30 AM and 1:30 PM, which is the approximate local time of the Aura-MLS measurements (for about 60°S to 60°N). Some climatologies have been produced by scaling measurements to sunrise/sunset for better comparison with occultation instruments.

$$\frac{\mathrm{VMR}^{\mathrm{observed}}(\text{corrected LST})}{\mathrm{VMR}^{\mathrm{model}}(\text{corrected LST})} = \frac{\mathrm{VMR}^{\mathrm{observed}}(\text{LST of observation})}{\mathrm{VMR}^{\mathrm{model}}(\text{LST of observation})} \tag{7.1}$$

The scaling to the corrected local solar time is done profile-by-profile, i.e. before averaging. For most instruments, the scaling uses lookup tables calculated from a photo-chemical box model initialised with climatological inputs. OSIRIS scaling factors (for NO_2) are obtained from a photochemical model initialised with measured trace gas abundances and temperature.

8 Summary and Conclusions

In this document, the algorithms applied to retrieve the products and climatologies to be delivered after Phase 1 of the SPARC Initiative have been described. The quality of the data is addressed in the Product Validation Report.